RESEARCH ARTICLE

Inter-decadal trends in the annual cycles of atmospheric CO_2 at Mauna Loa

K. S. Yajnik* and P. S. Swathi

CSIR Centre for Mathematical Modelling and Computer Simulation, NAL Belur Campus, Wind Tunnel Road, Bangalore 560 037, India

Cyclical rise and fall of monthly mean CO_2 concentration occurred rather regularly at Mauna Loa, Hawaii, USA, during 1958–2008, with peaks occurring in April or May followed by troughs in September or October. However, the frequency of troughs in September increased from 32% in 1958–1974 to 82% in 1992–2008 and the depletion season correspondingly decreased from 4.8 months on average to 4.2 months. Does this seemingly small change in the seasonal rhythm point to changes on an inter-decadal scale in the CO_2 accumulation rates? This question is studied here by examining linear and exponential trends of seasonal and annual CO_2 accumulation rates in three equal phases (1958–1974, 1975–1991 and 1992–2008). We also discuss trends of average accumulation rates in the accretion and depletion seasons, and of the amplitude and standard deviation of the annual CO_2 cycles at Mauna Loa, which can be viewed as representative of the North Central Tropical Pacific.

Keywords: Annual cycles, atmospheric carbon dioxide, industrial emissions, inter-decadal trend.

THE time series record of atmospheric CO_2 observations at Mauna Loa (19.5N, 155.6W; 3397 m; Mauna Loa (MLO), Hawaii), has long served as a focal element in most of the quantitative inferences on the secular increase of atmospheric CO_2 and associated variations of CO_2 fluxes. In its first decade, it provided direct evidence of secular increase and a seasonal variation, whose amplitude increases with latitude[1,2]. Observations in the subsequent decades along with isotopic measurements showed the seasonal CO_2 cycle to be closely correlated with terrestrial vegetation cycle in the northern hemisphere, and the long-term annual increase to be correlated with industrial CO_2 emissions. Indeed it was inferred that vegetation activity had increased peak to trough variation of seasonal change between 1964 and 1994 by ~20% (ref. 3). Also, extreme values of annual CO_2 increase variations were found to be correlated with El Nino events and volcanic eruptions[4]. Furthermore, quantitative inferences from the observational records have been used for developing a three-dimensional atmospheric model for CO_2 transport and, in more recent times, in developing inverse methods for determining regional carbon emissions from CO_2 measurements at a global network of observational sites[5]. It would not be an exaggeration to say that the Mauna Loa record has been the cornerstone in shaping the present knowledge of the carbon cycle.

Nearly continuous CO_2 measurements at Mauna Loa carried out by the Scripps Institution of Oceanography (SIO), USA, are based on absorption of infrared light from a dried sample of air drawn from a location upwind of the laboratory. Use of frequent calibration with working standard gases ensures accuracy and reliability. Remoteness of the site assures *a priori* that the effects of vegetation and human activities are minimal. But upwind effects of distant sources do occur in the afternoon and downwind effects in the late evening. Contamination effects also occur during local volcanic eruptions. Protocols have been devised, and tested repeatedly, to exclude measurements contaminated by local disturbances from the sample used for determining first daily average and subsequently monthly average[2,6,7]. Working standard gases have been calibrated repeatedly over time with primary standard gases maintained in the SOI Standards Laboratory. These exercises have led to several corrections for drift in calibration[8]. Numerous back-up studies on identification and elimination of systematic errors and calibration errors have enhanced confidence in the monthly mean record, which has a resolution of 0.01 ppm and an estimated accuracy/imprecision about 0.1 ppm, as the quantitative indicator of the state of large mixed air masses above the planetary boundary layer in the North Central Pacific[6]. When one deals with a dataset obtained over ~ 50 years, it is but natural to wonder about possible errors arising from various sources such as transition from analogue to digital instruments and from manual to automatic data processing, and evolutionary changes in calibration and other protocols. Some indication can be obtained from comparison with nondispersive infrared measurements carried out at Mauna Loa by the National Oceanographic and Atmospheric Administration (NOAA, USA), using instruments and data-analysis procedures that are distinct from SIO. Corresponding monthly mean CO_2 values of the NOAA and SIO datasets over 1974–1985 were found to differ on average by 0.15 ppm, with a standard deviation of 0.18 ppm (ref. 9).

The overall strategy of data analysis adopted by Keeling and co-workers is to suppress diurnal cycle for obtaining data representative of a broad area and to consider

*For correspondence. (e-mail: ksy@cmmacs.ernet.in)

Table 1. Representations of oscillatory and secular components in the analyses of Mauna Loa CO_2 data

Reference	Oscillatory component	Secular component	Range	Standard error (ppm)
10	$Q_1\sin 2\pi t + Q_2\cos 2\pi t + Q_3\sin 4\pi t + Q_4\cos 4\pi t$	$Q_5 + Q_6 t + Q_7 t^2 + Q_8 t^3$	1958–72	0.27
11	$Q_1\sin 2\pi t + Q_2\cos 2\pi t + Q_3\sin 4\pi t + Q_4\cos 4\pi t$	$Q_5 + Q_6 t$	1958–62	
8	$(1+\alpha t)\sum_{k=1}^{K}[A_k \sin(2\pi k t) + B_k \cos(2\pi k t)]$	$C_1 + C_2\exp(C_3 t)$	1958–82	0.23
6	$(1+\gamma t)\sum_{k=1}^{m}(a_k \sin\omega_k t + b_k \cos\omega_k t)$	$C_1 + C_2\exp(C_3 t) + R + \overline{\varepsilon_{\text{obs}}}(t)$	1958–85	0.35
12	$(1+\gamma t)\sum_{k=1}^{m}(a_k \sin\omega_k t + b_k \cos\omega_k t)$	C_{annual}	1958–2000	0.36

Notation in the above relations is the same as in the references. $Q_{1,\ldots,}Q_8$, $C_{1,\ldots,}C_3$, A_k, B_k, a_k, b_k, α and γ are constants whose values are determined by curve fitting. K and m are at most 4, and $\omega_k = 2\pi kt$. R is a spline function and $\overline{\varepsilon_{\text{obs}}}$ is the experimental noise. C_{annual} is an exponential plus a stiff spline. Time t is measured in years with origin taken at 1957.

monthly means so that synoptic variations due to individual weather events are excluded. Furthermore, a seasonal residual is removed from observations to obtain interannual variations that are expected to be approximately globally uniform[6]. Thus most of quantitative inferences drawn from Mauna Loa monthly mean CO_2 data are based on decomposition of CO_2 concentration into a seasonal oscillatory part and a secular part. In the earlier works, the seasonal component was taken to be annually periodic with at most four harmonics whose amplitudes and phases were determined by least square procedure. After mid-eighties, when it became clear that the seasonal CO_2 cycle has a distinct increasing trend, a common linearly increasing trend was assumed for the amplitudes of all the harmonics. The secular part was initially taken to be a polynomial with a spline function to accommodate interannual variations and, in later years, an exponential trend replaced the polynomial trend (Table 1). Extensive discussions of procedures can be found in several papers by Keeling and coworkers[6,8,10–12].

As global carbon transport models developed, there was a need for integrating data from continuous monitoring stations, flask-based land-based stations and ship-based positions into a database which can be used for estimating the sources and sinks on the earth surface by inverse methods. Masarie and Tans[13] have given the basic curve-fitting procedure that is now widely used. Most of its differences from the procedures described earlier stem from the need to deal with two categories of data differing markedly in sampling frequency. For example, the procedure uses daily mean data from a continuously monitoring station and fits a quadratic function with four harmonics with constant amplitude and phase, as in Keeling *et al.*[10] (see Table 1), to generate a site climatology for the given period (in the case described in the paper[13], 1979–1994). A smooth curve is then obtained by digitally filtering the residual of the data with respect to the climatology with a low-pass filter with a 40-day cut-off and then adding it to the site climatology. A 'deseasonalized long-term trend' is obtained by digitally filtering the residual with a low-pass filter with a 1-year cut-off and then adding it to the quadratic function[13,14].

Methodology

It is expedient to introduce first the notation. Let C_{nm} denote the mean CO_2 concentration (dry fraction in ppm by volume) of the mth month of the nth year (m = 1, 2, ..., 12, and n = calendar year – 1957), and a two-digit format is used in specifying numerical value of either subscript. Let $C_n^{\max}$ and $C_n^{\min}$ denote the peak (maximum) and trough (minimum) in the nth year. Figure 1 *a* explains the notation in the context of the annual CO_2 cycles at Mauna Loa during 2004–2008 (ref. 15).

The annual peak occurs in either April or May and the annual trough in either September or October during the entire period (1958–2008), except for two years of missing data (January and February in 1958, and February to April in 1964). We assume that the same pattern holds for 1958 and 1964. Furthermore, as the mean CO_2 concentration of April 1964, C_{0704}, is determined here by linear interpolation from C_{0604} and C_{0804}, and is less than C_{0705}, the peak in 1964 occurs in May. Figure 1 *b* shows the months of peaks and troughs. (The location of the trough at 9.5 in 1967 indicates that CO_2 concentrations in September and October are equal.)

Table 2 shows the frequency of the months of the peaks and troughs in the period 1958–2008 as a whole and in the three phases. The frequency of troughs in September increases dramatically from 32% in phase I to 82% in phase III, and the average length of the depletion season (peak-to-trough) decreases from 4.8 to 4.2 months. These changes indicate a subtle transition on an inter-decadal scale in the seasonal rhythm of the carbon cycle in the North Central Tropical Pacific. It also points to the possi-

bility that the behaviour of the annual cycle might not be homogeneous over the entire period 1958–2008. In particular, it leads to the question: Are there are any significant variations on the inter-decadal scale in seasonal or annual CO_2 accumulation rates or in annual cycle parameters? This question is investigated here by dividing the period 1958–2008 into three phases of equal duration, and examining trends in accumulation rates and annual cycle parameters in the three phases. Our methodology differs from earlier approaches in two ways. First, we focus on the accumulation rate of CO_2, also called CO_2 tendency, rather than CO_2 concentration, as the former can be related to the net influx into the region. Second, we consider annual cycles that include variations on all timescales instead of seasonal cycles, which are restricted to variations on seasonal timescales. Consequently, we do not need to decompose CO_2 variation into seasonal and aseasonal (interannual and secular) parts.

When photosynthetic uptake of CO_2 by terrestrial vegetation exceeds the threshold of respiration plus industrial emissions plus other emissions such as wild fire and transport, net influx into the region becomes negative resulting in CO_2 depletion. If the depletion season is defined as the season of negative accumulation rate, which begins from the month of the peak and ends in the month of the trough, the average drawdown rate in the season would be $(C_n^{max} - C_n^{min})/T_n^{dep}$, T_n^{dep} being the length of nth year depletion season. If we define the other (accretion) season as one of positive accumulation rate, it begins when the monthly mean CO_2 is the lowest in the previous calendar year and ends when it peaks in the current year. The average accumulation rate in the accretion season would then be $(C_n^{max} - C_{n-1}^{min})/T_n^{acc}$, T_n^{acc} being the duration of the season.

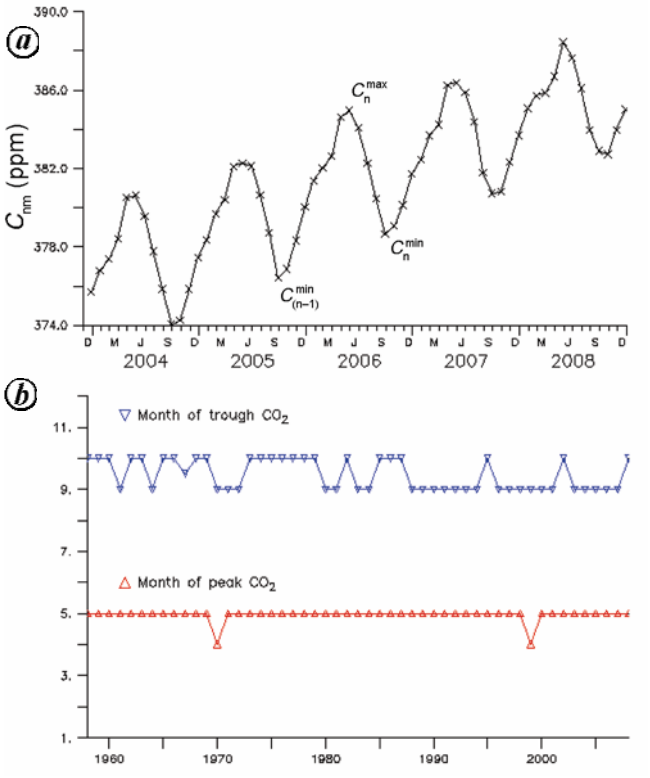

Figure 1. ***a***, Annual CO_2 cycles at Mauna Loa in 2004–08 and definition sketch. ***b***, Months of peaks (red triangles) and troughs (blue triangles) in 1958–2008. C_{nm} denotes monthly mean concentration of CO_2 (dry fraction, ppm) in the mth month of the nth year (n = calendar year – 1957). Superscripts max and min denote peak (maximum) and trough (minimum), and subscript n denotes the year. Monthly mean CO_2 data for all figures and tables have been sourced from the CDIAC website[15].

It is customary to define seasons of constant duration. Such an alternative definition of the depletion season would then be from 1 May to 30 September, and the accretion season from 1 October of the previous year to 30 April of the current year. The average drawdown rate, with the alternate definition, would then be $(C_{n04} + C_{n05} - C_{n09} - C_{n10})/(5T/6)$ ppm yr^{-1} for the depletion season, and $(C_{n04} + C_{n05} - C_{(n-1)09} - C_{(n-1)10})/(7T/6)$ ppm yr^{-1} for the accretion season. (Although we use the standard calendar, all months and all years are taken to be equal to simplify analysis; T is one year.) Note that this definition suppresses the change in the annual rhythm mentioned earlier. It also has a smoothing effect.

Annual CO_2 accumulation rate may be defined as the average rate of increase of CO_2 concentration in a calendar year $(C_{(n+1)01} + C_{n12} - C_{n01} - C_{(n-1)12})/2T$, or in the running year from the middle of the current month of the current year to the middle of the same month of the following year $(C_{(n+1)m} - C_{nm})/T$. In either case, it is approximately a weighted average of drawdown rate in the depletion season(s) and accumulation rate in the accretion season(s) in the year. The second definition however has one major advantage over the first, as it provides an order of magnitude larger sample for determining inter-decadal trends. But if we wish to compare the inter-decadal trends based on the two definitions, we need a rule to determine the phase to which a given running year is assigned. Our calculations are based on the following rule. A running year is assigned to phase I, II or III, depending on which has more than 6 months of the running year. Consequently, running years beginning prior to July 1974 are assigned to the phase I (1958–74), years starting after July 1974 but before July 1991 to phase II, the years beginning after July 1991 to phase III (1992–2008), and two years, one beginning in July 1974 and the other in July 1991 are left unassigned and are not considered in the trend analysis.

In the determination of trends, we use local time by shifting the origin of the time axis to the midpoint of the phase or the period. Such a choice of origin has the major advantage that the intercepts of the linear and exponential trends are then equal to arithmetic and geometric means respectively. The equality is exact if the axis is exactly midway and if there are no missing data points; otherwise, it is approximate. This property facilitates interpretation of the value of the intercepts. Trend parameters are determined by minimizing the sum of

Table 2. Frequency of peaks and troughs of the annual CO_2 cycle at Mauna Loa[15]

Period	1958–2008	1958–1974	1975–1991	1992–2008
Phase		I	II	III
No. of years	51	17	17	17
Peaks in April	2 (4%)	1 (6%)	0 (0%)	1 (6%)
Peaks in May	49 (96%)	16 (94%)	17 (100%)	16 (94%)
Troughs in September	27.5 (54%)	5.5 (32%)	8 (47%)	14 (82%)
Troughs in October	23.5 (46%)	11.5 (68%)	9 (53%)	3 (18%)
Average depletion season (month)	4.5	4.8	4.6	4.2
Average accretion season (month)	7.5	7.2	7.4	7.8

squares of errors (SSE) for the linear trend and the sum of squares of errors in logarithms (SSEL) for the exponential trend. Consequently, if the seasonal or the annual accumulation rate is zero or negative, such data are to be ignored in the present work for determining the exponential trend and the data point is treated as a missing one.

When the linear trend rate is small, is there any need to determine the exponential trend? The linear trend parameters are known to be sensitive to large deviations from the trend. On the other hand, minimization of SSEL makes the exponential trend rate parameters much less sensitive to large deviations. In the present case, CO_2 accumulation rates show large inter-annual variations with dominant frequency of 2–4 years due to well-known ocean–atmosphere oscillations in the equatorial Pacific, which lead to large deviations from the trend curve. Therefore, comparison of parameters of linear and exponential trends indicates the parameter sensitivity to large deviations. There is also the option of using the first two terms of the Taylor series expansion of the exponential trend as a linear trend with alternate values of trend parameters. In what follows, parameters of linear and exponential trends are given in Tables 3 and 4, but only linear trend curves are shown in figures 2 and 3 when the trend rates are small and the linear and exponential trends are not far enough to be easily distinguishable.

Results and discussion

The average drawdown rate for the depletion season is shown in Figure 2 *a*, and the average accumulation rate in the accretion season in Figure 2 *b*. Black crosses indicate results for variable duration seasons (VDS) and red circles for constant duration seasons (CDS). The drawdown rate in the depletion season is lower for CDS than for VDS, as the CDS numerator is smaller and denominator is larger. On the other hand, the accumulation rate in the accretion season for CDS is lower in the earlier years than VDS but higher in the subsequent years, as both the numerator and the denominator are smaller in CDS than VDS. Also, the drawdown of CO_2 in the shorter depletion season is not sufficiently rapid to compensate accumulation in the longer accretion season in any year. Consequently, there is a net increase in CO_2 concentration in all years during 1958–2008.

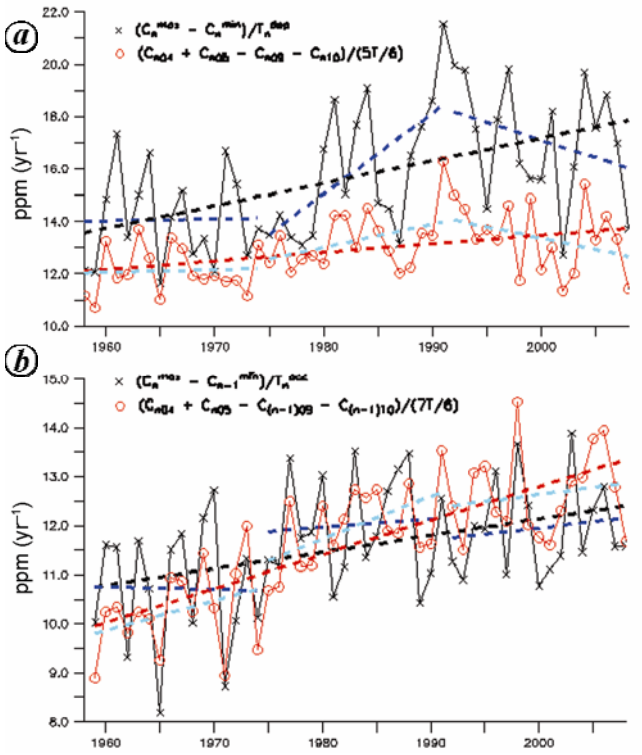

Figure 2. Drawdown/accumulation rates of atmospheric CO_2 at Mauna Loa averaged over (***a***) depletion season and (***b***) accretion season according to two definitions. Black crosses indicate variable duration seasons (VDS, peak-trough and trough-peak) and red circles constant duration seasons (CDS, May–September and October–April). Dashed lines show linear trends, black for the entire period and blue for phases I–III in the case of VDS, and red and light blue in the case of CDS. T_n^{dep} and T_n^{acc} denote the lengths (in years) of the depletion and accretion seasons of the *n*th year in the case of VDS. In the case of CDS, the lengths of the seasons are 5/12 and 7/12 yr. Remaining notations are as in Figure 1 *a*. See Table 3 for intercepts, and linear and exponential trend rates.

Linear trend lines are shown in Figure 2 *a* and *b* by short dashes in black for VDS and in red for CDS for the entire period, and in blue and light blue for the three phases. Exponential trend curves are not shown, as they are close to the linear trend lines. Both definitions of season give qualitatively similar trends for the drawdown rates in the depletion season: negligible trend rate in the first phase, an increasing trend in the second and a decreasing trend in the third. So one can conclude that the CO_2 drawdown rates in the depletion season were

Table 3. Inter-decadal trends in annual CO_2 cycles at Mauna Loa[15]

	Intercept[a]				Trend rate[b] (% yr^{-1})			
Period	1958–2008	1958–1974	1975–1991	1992–2008	1958–2008	1958–1974	1975–1991	1992–2008
Average drawdown rate of CO_2 in depletion season (Figure 2 *a*)								
Variable duration season (peak–trough)								
LT	15.71	14.07	15.97	17.09	0.55	0.05	1.92	–0.78
ET	15.52	13.97	15.79	16.95	0.55	0.09	1.88	–0.79
Constant duration season (May–September)								
LT	12.92	12.12	13.28	13.36	0.26	0.06	0.55	–0.65
ET	12.87	12.09	13.24	13.31	0.25	0.10	0.63	–0.67
Average accumulation rate of CO_2 in accretion season (Figure 2 *b*)								
Variable duration season (trough–peak)								
LT	11.56	10.73	12.01	11.95	0.29	–0.05	0.14	0.25
ET	11.49	10.65	11.97	11.92	0.31	–0.06	0.13	0.21
Constant duration season (October–April)								
LT	11.62	10.23	11.96	12.64	0.59	0.59	0.73	0.23
ET	11.55	10.20	11.96	12.61	0.61	0.56	0.74	0.23
Annual CO_2 cycle parameters (Figure 3)								
Amplitude								
LT	2.90	2.75	2.97	2.99	0.21	–0.18	0.71	–0.58
ET	2.89	2.74	2.96	2.98	0.21	–0.16	0.67	–0.57
Standard deviation								
LT	1.85	1.76	1.90	1.90	0.19	0.18	0.43	–0.64
ET	1.84	1.75	1.89	1.89	0.19	–0.17	0.40	–0.63
Calendar year average CO_2 accumulation rate (Figure 4 *a*)								
LT	1.41	0.91	1.50	1.83	1.90	3.64	0.39	2.86
ET	1.27	0.81	1.43	1.72	2.20	4.24	0.24	3.73
Running year average CO_2 accumulation rate (Figure 4 *b*)								
LT	1.41	0.94	1.49	1.79	1.79	3.56	0.56	2.53
ET	1.24[c]	0.83[c]	1.40	1.63	2.00[c]	2.80[c]	0.31	3.70

LT, Linear trend; ET, Exponential trend. [a]If the linear trend is given by $a + b(t - c)$, and the exponential trend is given by a*exp($b(t - c)$), a is the intercept. The origin of the time axis is on 1 January 1957, $c = 9$ for phase I, 26 for phase II and the entire period, and 43 for phase III. The units of intercept are ppm yr^{-1} for Figures 2 and 4, and ppm for Figure 3. [b]Trend rate is, in the above notation, 100*b/a in the linear trend and 100*b in the exponential trend. [c] One instance of zero value and seven instances of negative values of annual accumulation rate in 1958–74 make these values anomalous (see the text for explanation).

essentially stable up to early 1970s, but subsequently they started increasing on an inter-decadal timescale, but after early 1990s, they had a decreasing trend. But so far as the accretion season is concerned, the two definitions do not present qualitatively similar trends for the accumulation rate, making it difficult to draw any conclusion. Note that the intercepts for linear and exponential trends agree within 0.2 ppm yr^{-1} and the trend rates within 0.1% yr^{-1} (Table 3).

Before analysing the annual accumulation rates of CO_2, let us consider two parameters of the annual cycle, namely the amplitude and standard deviation. We define here the amplitude as half of the peak-to-trough value, which is a generalization of what is used for a sine wave. (Some authors define the amplitude as the peak-to-trough value, that is, annual maximum–annual minimum, which would be ordinarily termed as annual range.) When the annual cycle has several harmonics, amplitude, unlike standard deviation, depends on the amplitudes of the harmonics as well as their phases.

Figure 3 shows the variation of two parameters (amplitude: black diamonds, standard deviation: red squares) and their linear trends for the three phases as well as 1958–2008 (Table 3). Their behaviour is rather similar to the average drawdown rate in the depletion season (Figure 2 *a*): low trend rate in phase I, a larger positive linear trend rate in phase II and a comparable negative trend rate in phase III. Thus Figures 2 *a* and 3, viewed together, suggest that the seasonal rhythm is in a quasi-equilibrium state on inter-decadal timescales in phase I, it has an increasing trend in phase II and a decreasing trend in phase III.

The annual CO_2 accumulation rates at Mauna Loa are shown for calendar year in Figure 4 *a* by crosses and for running year in Figure 4 *b* by circles. Numerical values of intercept (in ppm yr^{-1}) and trend rates (in % yr^{-1}) are given in Table 3.

Table 4. Comparison of linear and exponential trends at Mauna Loa with four SIO sites based on running year CO_2 accumulation rates[15]

	1958–2008	1958–1974	1975–1991	1992–2008
CO_2 accumulation acceleration rate (linear trend rate, ppm $yr^{-2} \times 100$)				
Mauna Loa, Hawaii (1958–2008)	2.52	3.36	0.84	4.50
South Pole, Antarctica (1958–2007)	2.64	2.48	0.58	5.15
Point Barrow, Alaska (1974–2007)			2.97	7.44
La Jolla Pier (1969–2007)			1.18	7.35
Christmas Island (1972–2007)			1.08	3.70
Doubling time for CO_2 accumulation rate (yr)				
Mauna Loa (19°32′N, 155°35′W)	35[a]	25[a]	220	19
South Pole (89°59′S, 24°48′W)	26	13	150	19
Point Barrow (71°19′N, 156°36′W)			52[b]	10
La Jolla Pier (32°9′N, 117°3′W)			89	12
Christmas Island (2°00′N, 157°18′W)			81	27

[a]See footnote [c]in Table 3. [b]Two instances of zero value and six instances of negative value of annual accumulation rate at Point Barrow in 1980 affect this value; five of such data points have values < –0.5 and are not shown in Figure 5.

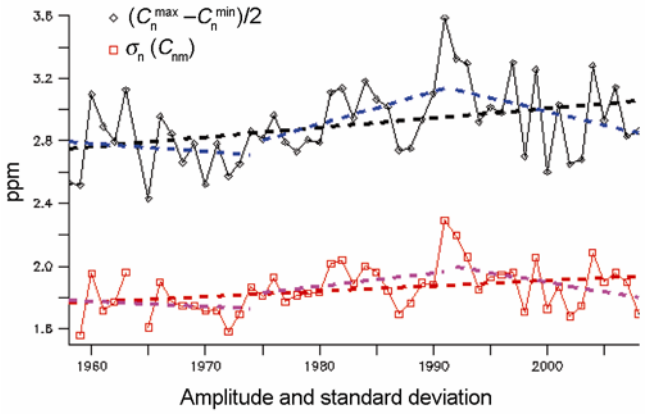

Figure 3. Trends of the parameters of the annual CO_2 cycle at Mauna Loa. Black diamonds indicate amplitude and red squares standard deviation. Linear trend lines are shown by short dashes. They are in black for the entire period, and in blue for the three phases for the amplitude and in red and light blue respectively for the standard deviation. Intercepts and trend rates are given in Table 3.

We first note that CO_2 accumulation rates for calendar year and running year have similar trends (Figure 4). Intercept values for calendar year and running year given in Table 3 agree within < 0.1 ppm yr^{-1} and trend rate values within < 0.4% yr^{-1} (anomalously low running year exponential trend rate and intercept in phase I are due to the increase in missing data points from 8 to 16 by one instance of zero value and seven instances of negative value of annual accumulation rate in 1958–1974 in a sample of 204; the effect is less significant for intercept and trend rate values for 1958–2008 due to the larger sample size; see Figure 4 *b*).

It is noteworthy that, for linear as well as exponential trends, the intercepts in phase III are nearly twice their value in phase I. Intercepts at the central axis being approximately equal to arithmetic or geometric means, the accumulation process of CO_2 in the atmosphere at Mauna Loa shows a strong tendency to accelerate on inter-decadal timescales. Trend rates, linear and exponential, can then be viewed as metrics of the acceleration tendency within a phase.

While linear and exponential trend rates for annual CO_2 accumulation rate in phase I are comparable with those in phase III, the trend rates for phase II are found to be markedly lower – by a factor of nearly one-fifth in the case of linear trends and by nearly an order of magnitude in the case of exponential trends (see the second column from the right in the last four rows in Table 3). So the inter-decadal scale acceleration of CO_2 accumulation has a high–low–high pattern. The low is so low that it may well be called a lull.

This remarkable result came to us as a surprise. It raised the question as to what could be the cause of a lull on an inter-decadal timescale in the acceleration of the accumulation of atmospheric CO_2. But before taking up the issue further, let us recall that Keeling[6] had observed earlier that the annual average CO_2 varies little (~ 3 ppm) across the globe. The implication is that the annual accumulation rate of CO_2 measured at Mauna Loa is expected to be a good approximation of the annual accumulation rate of the global average. If that is so, then the lull in acceleration during 1975–1991 observed at Mauna Loa is a manifestation of a global lull. But is there any evidence to support this expectation?

Figure 5 shows the running year CO_2 accumulation rates obtained from four datasets of atmospheric CO_2 based on air-flask samples (2–3 per week) collected at four sites of SIO that go at least as far back as mid-seventies (blue crosses for Point Barrow, Alaska; light blue square for La Jolla Pier, California; red rhombus for Christmas Island, and black crosses for South Pole, Antarctica)[15]. Intercepts and trend rates were determined for

phases II and III for all the four sites, and additionally for phase I and for 1958–2008 for the South Pole by applying the same running year method as was used for Mauna Loa. For the sake of clarity, linear trends are given in Figure 4 *a* and exponential trends in Figure 4 *b*. Linear trend rates (ppm yr^{-1}) and doubling times for exponential trends are given in Table 4 along with the results for Mauna Loa.

Low time resolution of flask-based measurements does not provide the kind of opportunities for identifying and removing data contaminated by effects of local sources and sinks as nearly continuous measurements. We also need to take into account that the CO_2 concentration datasets for the four sites are obtained by fitting a curve consisting of four harmonics plus a stiff spline and a linear gain factor. The tabulated values correspond to the 15th day of each month. This process filters out high-frequency components, which results in smoother variations in Figure 5 than in Figure 4. Furthermore, it should be clear from the remarks on such procedures in the introduction that systematic errors may be introduced unintentionally by the procedure itself. So the differences one sees in the trends in Figure 5 and the values of linear trend rates in Table 5 are in part due to these factors. Despite these differences, it is clear that linear trend rates are significantly lower and doubling times for exponential trends significantly larger in phase II than in phase III at all the four sites. Thus it is reasonable to conclude on the basis of this evidence that the acceleration of CO_2 accumulation on an inter-decadal timescale had a global lull in 1975–1991. Further verification is undoubtedly needed using datasets of other atmospheric CO_2 observation sites along with systematic cross-comparison of inter-decadal trends.

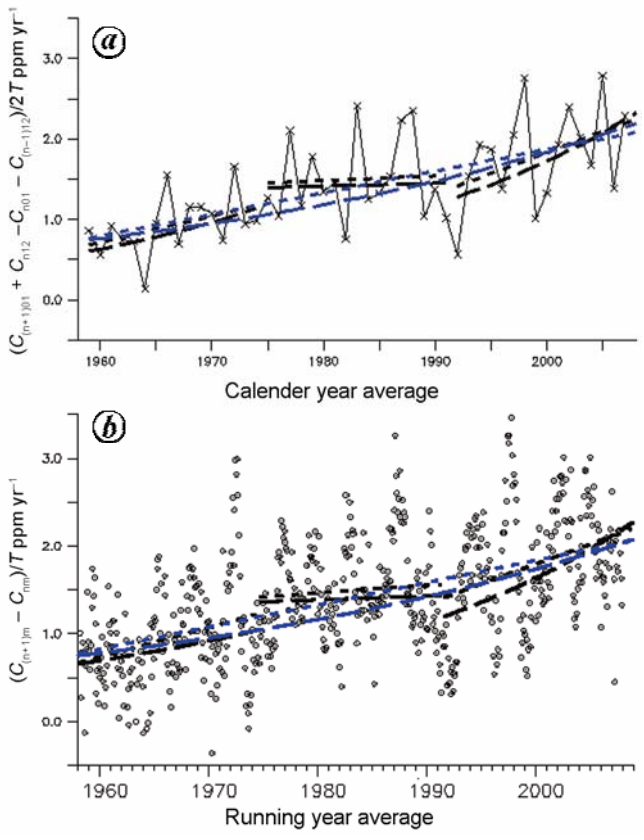

Figure 4. Inter-decadal trends of annual CO_2 accumulation rate. Calendar year average rates are shown with crosses in (***a***) and running year average rates with circles in (***b***). Linear trends are shown with short dashes and exponential trends with long dashes for 1958–2008 in blue and for the three phases in black. Intercept and trend rates are given in Tables 3 and 4. Note the strikingly lower trend rates in phase II (1975–91).

Now let us return to the question of possible causes for a global lull in acceleration of atmospheric CO_2. Variations due to known atmosphere–ocean oscillations on basin-scale tend to be cyclic and have smaller timescales. Episodic phenomena like volcanic eruptions, etc. have transient regional effects. There are, to the best of our knowledge, no known natural processes or phenomena that can account for such a marked slowdown. Could then the lull be due to anthropogenic effects and, in particular, industrial emissions?

Let us now look at the economic evidence based on the recent analysis of the history of oil shocks by Hamilton[16]. The US economy had eight recessions of during 1958–2008. All but one were associated with one or two episodes of sharp rise in oil prices, the solitary exception being in 1960. Half of these recessions occurred between November 1973 to December 1991 (their beginning dates, as determined by the National Bureau of Economic Research, are November 1973, January 1980, July 1981 and July 1990). Corresponding oil price rise episodes were in April–September 1973 (16%) and November 1973–February 1974 (51%), May 1979–January 1980 (57%), November 1980–February 1981 (45%), August 1990–October 1990 (93%). They were also correlated with major geopolitical events in the Middle East (OPEC Embargo, Iranian revolution, Iran–Iraq War and Gulf War I).

Clearly, one can argue on the basis of the observations of Hamilton that increased political and economic uncertainties in this period made risk assessment extremely difficult, thereby inhibiting investments, the unintended consequence being markedly lower increase of industrial emissions. On the other hand, the end of the Cold War brought about considerable relaxation in the international political climate facilitating risk assessment as well as compensation of the adverse economic effects of increased oil prices by massive shift of investment and manufacturing to low-wage economies. Resumption of growth of industrial emissions, one would further argue, was the unintended consequence. This argument, which is based on circumstantial economic evidence, leads to the inference that the rate of increase of industrial emissions was substantially subdued during 1974–1991. If so, it was

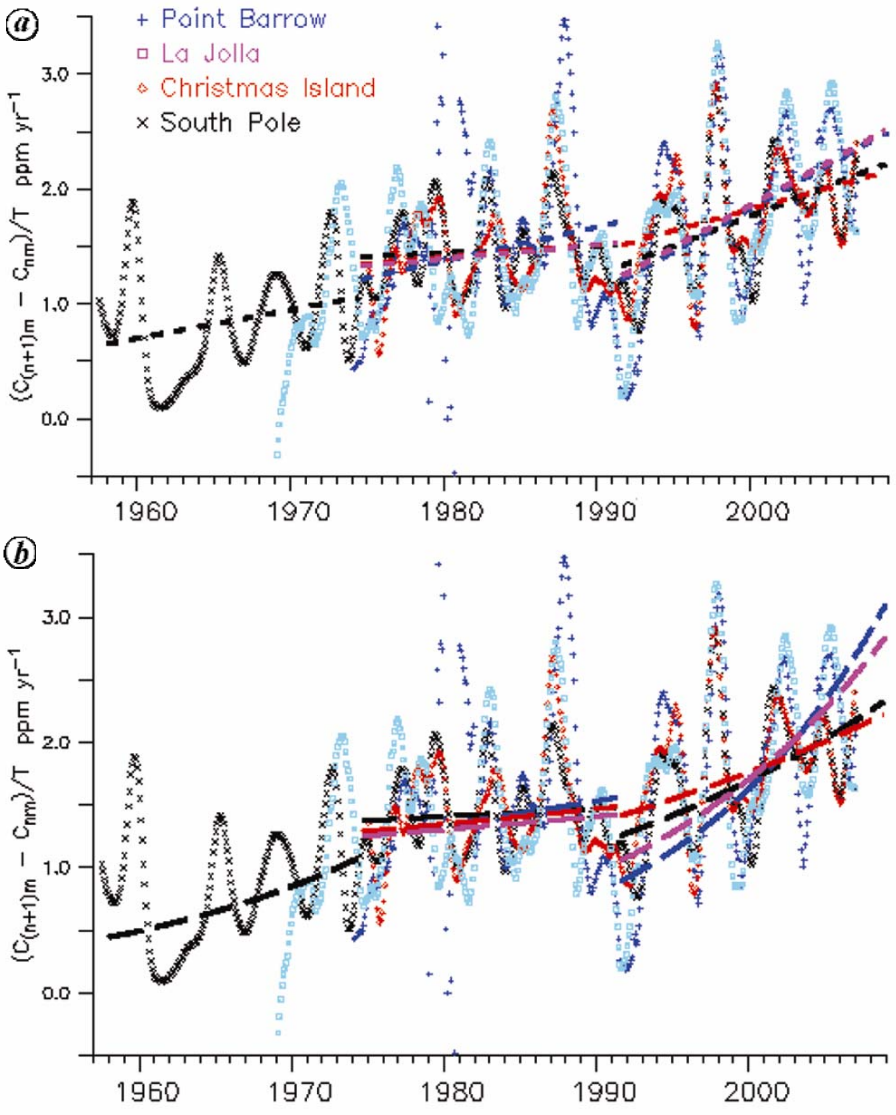

Figure 5. Running year average CO_2 accumulation rates at four SIO sites. Annual accumulation rates are shown for Point Barrow by blue crosses, for La Jolla Pier by light blue squares, for Christmas Island by red diamonds and for South Pole by black crosses. Linear trends are shown in (***a***) with short dashes, and exponential trends are shown separately for clarity in (***b***) with long dashes. Note the markedly lower trend rates in phase II for all the four sites.

probably the main contributing factor in the lull in the acceleration of CO_2 accumulation.

A few implications of the above argument are worth further examination. Linear trend rates of annual CO_2 accumulation for phase III are larger than those for phase I in absolute terms (in ppm yr^{-2}; see first two rows in Table 4) but smaller in relative terms (in % yr^{-1}; see second last and fourth last rows in Table 3). This would suggest that while average rate of increase in the industrial emissions rate was larger in 1992–2008 in absolute terms (GTC yr^{-2}), it was smaller in relative terms (% yr^{-1}), which is certainly expected in light of multitude of technological innovations and numerous governmental and non-governmental initiatives. Second, future projections based on extrapolations of ~50 yr trends would be simplistic. In particular, they could lead to serious overestimates of atmospheric CO_2 accumulation or equally serious underestimates depending on whether economic/political uncertainties and oil price increases in 2009–2025 are comparable to 1975–1991 or 1992–2008. Perhaps, the best course, based on the present understanding, seems to have two-truck approach of two alternate business-as-usual scenarios, one termed as optimistic and the other pessimistic in the context of climate change.

In summary, the present analysis of the observations at Mauna Loa during 1958–2008 reveal a high-low-high pattern in the acceleration on an inter-decadal timescale of atmospheric CO_2 accumulation. A lull is found to occur in 1975–1991, when linear trend rate of CO_2 accumulation rate fell to as low as one-fifth of its value in

1958–1974 and 1992–2008, and the doubling timescales of accumulation rate became nearly an order of magnitude larger. Similar calculations for four other atmospheric CO_2 observation sites suggest that the lull is global. Recent economic analysis of oil shocks[16] provides circumstantial evidence for an argument linking the lull with an episode of high economic and political uncertainties, beginning with the first oil shock and ending with the end of the Cold War. These results suggest potential utility of monitoring trend rates of running year average CO_2 accumulation rates on interdecadal timescales as indices of effectiveness of emission control measures in controlling the acceleration of CO_2 accumulation in the medium term.

1. Keeling, C. D., The concentration and isotopic abundances of carbon dioxide in the atmosphere. *Tellus*, 1960, **12(**5), 200–203.
2. Pales, J. C. and Keeling, C. D., The concentration of atmospheric carbon dioxide in Hawaii. *J. Geophys. Res*., 1965, **70**(24), 6053–6076.
3. Keeling, C. D., Chin, J. F. S. and Whorf, T. P., Increased activity of northern vegetation inferred from atmospheric CO_2 measurements. *Nature*, 1996, **382**, 146–149.
4. Keeling, C. D., Whorf, T. P., Wahlen, M. and van der Plicht, J., Interannual extremes in the rate of rise of atmospheric carbon dioxide since 1980. *Nature*, 1995, **375**, 666–670.
5. Gurney, K. R. *et al.*, Towards robust regional estimates of CO_2 sources and sinks using atmospheric transport models. *Nature*, 2002, **415**(6872), 626–630.
6. Keeling, C. D. *et al.*, A three-dimensional model of CO_2 transport based on observed winds: analysis of observational data. In *Aspects of Climate Variability in the Pacific and the Western Americas* (ed. Peterson, D. H.), Geophysical Monograph 55, American Geophysical Union, Washington DC, 1989, pp. 165–236.
7. Keeling, C. D. and Whorf, T. F., Atmospheric CO_2 derived from flask air samples at SIO network. In *Trends of Data on Global Change*, Carbon Dioxide Information Analysis Center, Oak Ridge National Laboratory, US Department of Energy, Oak Ridge, Tennessee, USA, 2004.
8. Bacastow, R. B., Keeling, C. D. and Whorf, T. P., Seasonal amplitude increase in atmospheric CO_2 concentration at Mauna Loa, 1959–1982. *J. Geophys. Res.*, 1985, **90**(D6), 10529–10540.
9. Komhyr, W. D., Harris, T. B., Waterman, L. S., Chin, J. F. S. and Thoning, K. W., Atmospheric carbon dioxide at Mauna Loa observatory 1. NOAA global monitoring for climate change measurements with a nondispersive infrared analyzer. *J. Geophys. Res. D*, **94**, 8533–8547.
10. Keeling, C. D., Bacastow, R. B., Bainbridge, A. E., Ekdahl Jr., C. A., Guenther, P. R. and Waterman, L. S., Atmospheric carbon dioxide variations at Mauna Loa observatory, Hawaii. *Tellus*, 1976, **6**, 538–551.
11. Keeling, C. D., The influence of Mauna Loa laboratory on the development of atmospheric CO_2 research. In *Mauna Loa Observatory 20th Anniversary Report* (ed. Miller, J.), NOAA Special Report, Washington DC, 1978, pp. 36–54.
12. Keeling, C. D., Piper, S. C., Bacastow, R. B., Wahlen, M., Whorf, T. P., Heimann, M. and Meijer, H. A., Exchanges of atmospheric CO_2 and $^{13}CO_2$ with terrestrial biosphere and Oceans from 1978 and 2000, SIO Reference 01-06 (Revised from SIO Reference No 00-21), Scripps Institute of Oceanography, San Diego, USA, 2001.
13. Masarie, K. A. and Tans, P. P., Extension and integration of atmospheric carbon dioxide data into a globally consistent measurement record. *J. Geophys. Res. D*, **100**, 11,593–11,610.
14. Thoning, K. W., Tans, P. P. and Komhyr, W. D., Atmospheric carbon dioxide at Mauna Loa observatory, 2, Analysis of the NOAA/GMCC data, 1974–1985. *J. Geophys. Res*., 1989, **94**, 8549–8565.
15. Keeling, R. F., Piper, S. C., Bollenbacher, A. F. and Walker, J. S., Scripps Institute of Oceanography, Univ. Calif., La Jolla, CA, USA, 2009, data accessed on 18 June 2010; http://cdiac.oml.gov./ftp/maunaloa-co2/maunaloa.co2
16. Hamilton, J. D., Historical oil shocks. In *Handbook of Major Events in Economic History*, 2010; http://dss.ucsd.edu/~jhamilto/oil_history.pdf accessed on 13 June 2011.

ACKNOWLEDGEMENTS. We thank the Ministry of Earth Sciences, Government of India for sponsoring the Project INDOMOD; Prof. P. Seshu, C-MMACS, Bangalore for providing the necessary facilities and R. P. Thangavelu and his colleagues in the Systems group for sustained support. We also thank the referee for useful comments.

Received 22 June 2011; revised accepted 24 January 2012